Particle-optical self-trapping

R. Gordon* and J. T. Blakely
Department of Electrical and Computer Engineering, University of Victoria, Victoria, British Columbia, Canada V8P 5C2

D. Sinton
Department of Mechanical Engineering, University of Victoria, Victoria, British Columbia, Canada V8W 2Y2

(Received 14 December 2006; revised manuscript received 9 February 2007; published 3 May 2007)

The formation of a self-guided beam pattern via optical trapping in a suspension of Rayleigh scatterers is studied. An analytic self-guided solution is presented that is valid for low intensities. A numerical solution of the coupled diffusion and optical-wave equations is presented, which shows an evolution toward a steady state that is independent of the initial optical beam shape. At higher intensities, the numerical solution shows the influence of higher-order nonlinearities, which lead to instability. We define a critical optical intensity, in terms of the particle size, refractive index contrast, and thermal energy, that characterizes the onset of higher-order effects. Instability is found that is consistent with past parametric studies of solitons.

DOI: 10.1103/PhysRevA.75.055801 PACS number(s): 42.65.Tg, 87.80.Cc

Optical spatial solitons are self-induced optical waveguides where a nonlinearity balances the natural diffraction of the optical beam [1]. The nonlinearities leading to these solitons have been effectively instantaneous, such as in the Kerr type [2], or slow to respond, such as in the photorefractive type [3]. Another effective Kerr medium is found in liquid suspensions of dielectric nanoparticles [4]. In that medium, optical trapping is used to introduce an effective nonlinear response. The gradient force in optical trapping [5] works against diffusion to concentrate the particles within the high-intensity region of a beam. This, in turn, influences the local refractive index and allows for optical waveguiding. Self-focusing and self-trapping of light have been demonstrated experimentally [6,7]. Figure 1 shows schematically how particle trapping forms a waveguide and that the trapping process is limited by diffusion and diffraction. The field of optofluidics has emerged from the combination of optics and microfluidics [8]. Recently, it has been shown that low-loss optical waveguiding may be achieved from nanosphere suspension stream within a microfluidic flow [9]. The presence of the nanospheres presents new opportunities for nonlinear optical functionality in fluid environments.

In this work, we present a theory of particle-optical self-trapping (POST). For the low-optical-intensity regime, an analytic POST solution is given. A numerical study, including both particle transport and the optical wave equation, is presented to demonstrate the evolution toward a steady state, which is independent of the initial optical beam distribution. At higher intensities, the numerical results deviate significantly from the analytic solution. A characteristic intensity, marks the onset of this deviation. Instabilities are found beyond the characteristic intensity, which agree with those presented in past parametric studies of solitons.

The equation governing particle transport in a continuous medium is given by

$$\frac{\partial C}{\partial t} = -\vec{\nabla}\cdot\vec{j}, \tag{1}$$

where C is the particle concentration and j is the associated flux. In the absence of transport via bulk fluid motion and electrophoretic effects, the flux may be expressed as

$$\vec{j} = -D\vec{\nabla}C + \nu\vec{F}C, \tag{2}$$

where D is the diffusion coefficient, ν is the mobility, and $\vec{F}$ is the sum of external forces acting on the particles. The Nernst-Einstein relation provides $\nu = D/(kT)$, where k is the Boltzmann constant and T the temperature.

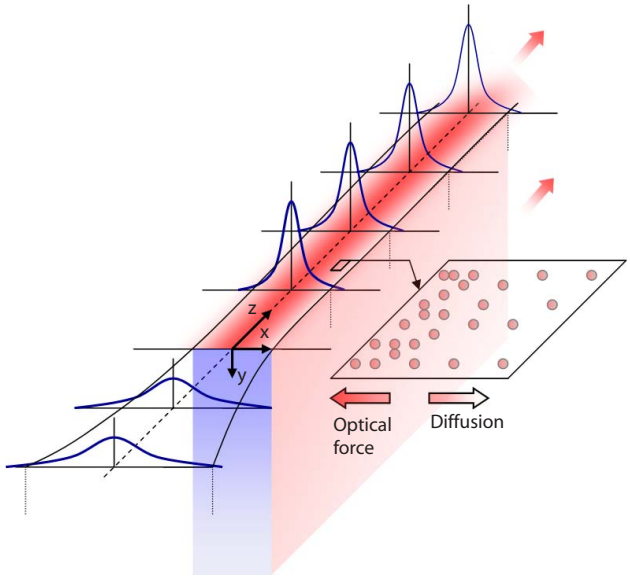

FIG. 1. (Color online) Schematic of particle-optical self-trapping (POST). The gradient in the local electric field intensity pulls the Rayleigh particles to the center of the beam. The resulting increase in the particle concentration serves to waveguide the light and further increase the trapping force on the particles. These processes are balanced by diffusion and diffraction, to give a steady beam geometry.

*Electronic address: rgordon@uvic.ca

The external force comes from the optical trapping force. The transverse component of the optical trapping force can be written as [5]

$$F_\perp = \frac{2\pi a^3}{c}\left(\frac{m^2-1}{m^2+2}\right)\vec{\nabla}_\perp I, \tag{3}$$

where a is the particle radius, c is the speed of light in a vacuum, m is the ratio of the refractive index of the particle (n_p) to the refractive index of the medium (n_m), $\vec{\nabla}_\perp$ is the transverse gradient, and I is the optical beam intensity. This force arises from the interaction of the induced dipole of a spherical Rayleigh scatterer (i.e., $a \ll \lambda$) with the gradient of the intensity. The parallel component of the force may also be suitably disregarded if the particles are replenished "upstream" so that there is no buildup, as has been done for L^2 waveguides [9]. Alternately, the parallel component of the force can be removed by having two counterpropagating optical beams of equal intensity, such as in an optical cavity [10], at the surface of a reflector, or with two collinear optical fibers [11].

Combining Eqs. (1)–(3) provides the transport equation for the particles:

$$\frac{\partial C}{\partial t} = D\nabla_\perp^2 C - \frac{2\pi a^3 D}{ckT}\left(\frac{m^2-1}{m^2+2}\right)\vec{\nabla}_\perp \cdot (C\vec{\nabla}_\perp I). \tag{4}$$

The wave equation governs the linearly polarized electric field:

$$\nabla^2\vec{E} = \frac{n^2}{c^2}\frac{\partial^2\vec{E}}{\partial t^2}, \tag{5}$$

where $\vec{E}$ is the electric field and n is the refractive index. We may choose a normalization for the electric field such that $I=|E|^2$, and so the electric field governs the particle transport through Eq. (4).

For Rayleigh scatterers of sufficiently low concentration ($C<0.1$) and with $m\sim 1$, the refractive index may be expanded as [4,9]

$$n^2 = n_m^2 + (n_p^2 - n_m^2)C; \tag{6}$$

thereby, the refractive index, which governs the electric field through Eq. (5), is determined by the particle concentration.

An obvious solution is provided for a plane-wave electric field distribution of constant transverse intensity and a uniform particle solution. It may be shown that this solution is subject to modulation instability by considering perturbations of the form $\exp(ik_x x+\gamma t)$, where k_x is the wave vector along the arbitrarily chosen transverse x direction, and the real part of γ is the exponential rate of growth. This result shows that any refractive index variations reorient the optical distribution and lead to more particle motion before diffusion takes effect.

The steady-state POST solution arises by setting $\partial C/\partial t = 0$, which allows the solution

$$C = C_0 \exp\left(\frac{I}{I_0}\right), \tag{7}$$

where C_0 is the background concentration of particles, and the critical optical intensity is given by

$$I_0 = \frac{ckT}{2\pi a^3}\frac{m^2+2}{m^2-1}. \tag{8}$$

For the case of $I<I_0$, so that $C\simeq C_0(1+I/I_0)$, and considering an electric field variation of the form $\vec{E} = \hat{y}A(x,y)\exp(ik_z z - i\omega t)$, Eqs. (4) and (5) give

$$\nabla_\perp^2 A - \Gamma^2 A + \Delta^2|A|^2 A = 0, \tag{9}$$

with $\Delta^2=(n_p^2-n_m^2)C_0\omega^2/(I_0c^2)$ and $\Gamma^2=k_z^2-n_m^2\omega^2/c^2-I_0\Delta^2$. This provides the one-dimensional spatial soliton solution:

$$A(x) = \frac{\sqrt{2}\Gamma}{\Delta\cosh(\Gamma x)}. \tag{10}$$

This continuum-based formulation does not account for individual particle fluctuations on the length scale of the wavelength of light in the medium, which arise from the small number of particles within each λ cube volume. However, over the length scale of the beam width ($\sim$10–100 μm), individual particle fluctuations do not contribute. The beam width is the smallest characteristic length scale in this problem; variations in the direction of propagation occur over a much larger length scale because of the small numerical aperture of the waveguide.

As both the diffusion and optical force terms in Eq. (4) depend on mobility, the relative strength of these effects shows no explicit dependence on diffusivity or viscosity, the latter being important only in the transient development of the steady-state solution. The optical and diffusive influences on the particles scale similarly with respect to length scale as well, and thus their relative strength shows no length-scale dependence, other than particle size. From a transport perspective, larger particles strongly favor optical focusing, as indicated by the cubic dependence on particle size in Eq. (8). The Rayleigh treatment in the analytic solution limits its applicability with respect to particle size. From the perspective of waveguiding applications, it is scattering effects that limit particle size [9].

We consider the numerical example of polystyrene spheres ($n_p=1.574$) of radius $a=50$ nm, suspended in water with negligible surfactant ($n_m=1.331$), and at room temperature. The free-space wavelength of light is chosen to be 1 μm, since there has been significant development of high-power laser diodes close to that wavelength. Given these parameters, it is found that $I_0=1.3\times10^{10}$ W/m^2. A 100 mW beam focused down to a 10 μm^2 area gives an intensity of 10^{10} W/m^2, which is comparable to I_0. Therefore intensity values close to I_0 should be easily obtained with even a single laser diode. Given a constant particle size, concentration in Eq. (4) may be interpreted directly as volume fraction. We consider the case of $C_0=0.01$, so that multiple optical scattering, and associated losses, may be suitably ignored.

Figure 2 shows the POST for the above parameters, as

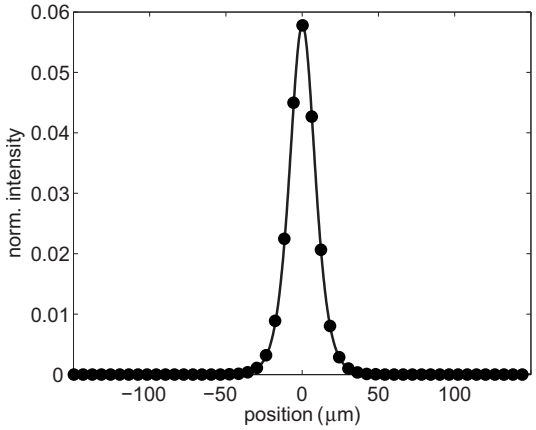

FIG. 2. POST solution Eq. (10) shown with solid line with maximum intensity normalized to I_0. Numerically calculated solution shown with dots (only 5% of the grid points used are shown).

described by Eq. (10), with a solid line. A numerical procedure was also developed to solve the dynamics of Eqs. (4) and (5), without the approximation of low field intensities. For comparison, Fig. 2 also shows the converged steady-state numerical solution with dots. For the numerical computation, the method of lines was used with a 300 nm spatial grid over 300 μm in the x direction, and the time integration was performed with an adaptive time-step fourth-order Runge-Kutta method. Perfect electric conductor boundary conditions were used for the y-polarized electric field, and circular boundary conditions were used for the particle concentration. The electric field adapts to the changes in the refractive index on time scales of the order of $n_m/(n_\delta\omega)$, where n_δ is a small refractive index difference from the increase in particle density in a region. Since ω is large, this is effectively instantaneous when compared with the time scale of the particle motion, which is of the order of a second for the tens of micrometer lengths involved. The dynamics are limited by the particle motion, and so the optical mode described by Eq. (5) adiabatically evolves with changes in the particle concentration. Therefore, the mode is assumed constant over time scales where there is little variation in the particle density, and then recalculated. In this procedure it was verified that the electric field intensity varies by less than 5% after each interval.

Figure 3 shows the evolution of the electric field [Fig. 3(a)] and particle concentration [Fig. 3(b)] toward the steady-state solution. The numerical solution evolved toward the self-trapped solution within a few hundred iterations. The similarity of these fields demonstrates the particle coupling. Figure 3(b) shows the additional feature of particle concentration depletion adjacent to the center of the beam. The solution showed no dependence on initial beam geometry, as different initial electric field distributions (Gaussian, sinusoidal, and exponential) of the same total power converged to the same final solution. The final solution converged stably in all cases tested in the range $I<1.4I_0$.

Figure 4 shows the ratio between the peak power and the total power as a function of the total power for both the analytic solution of Eq. (10), shown with a straight solid line, and the numerical calculations, shown with dots. The ratio of peak power to total power is a measure of the inverse optical

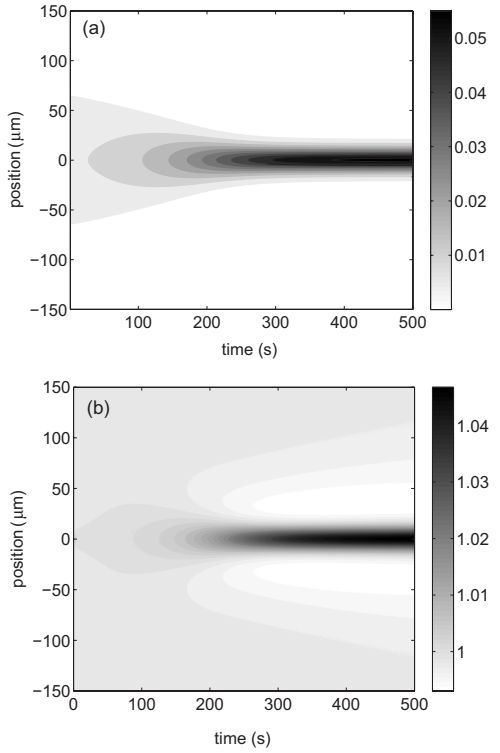

FIG. 3. Evolution of (a) electric field and (b) particle concentration to steady-state POST solutions for the same conditions as Fig. 2, found by solving Eqs. (4) and (5) numerically. Scale bars have been normalized to I_0 and C_0, respectively.

width. The inverse optical width was determined directly from the analytic POST solution, Eq. (10), to be proportional to total input power and to exhibit a slope of $\Delta^2/8$, as plotted in Fig. 4. The low-intensity regime corresponds to low peak intensities and large optical widths. The analytic solution is well suited to this regime when an infinite medium is considered.

The dashed line in Fig. 4 gives the boundary of peak intensity equal to I_0. As the input power and the resulting peak intensity are increased further, toward $I\sim I_0$, there is a

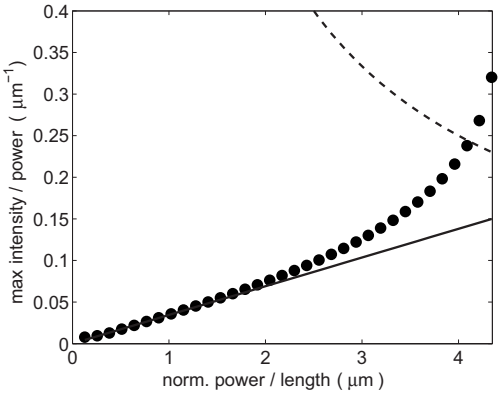

FIG. 4. Power dependence of POST. Ratio of peak intensity to total power as a function of total input power (normalized to I_0) from analytic POST solution of Eq. (10), shown with straight solid line, and from numerical calculations, shown with dots. Dashed line shows where the peak intensity is I_0.

deviation from the analytic solution. (The analytic solution contains only the first-order term in the Taylor expansion.) The numerical solution experiences a blowup instability for intensities where the analytic peak intensity is above $1.4I_0$. This instability agrees with instabilities found through parametric soliton studies on nonlinear refractive index variations of powers higher than 2 (i.e., I^2) [12]. For the highest-intensity stable POST, the last point shown in Fig. 4, there are still ten data points within the POST full width at half maximum, so spatial discretization is not the source of the instability. In practice, the maximum intensity resulting from instability will be limited by the natural saturation of the refractive index change due to the particulate nature of the system. Assuming hard-shell packing, it is required that $C < 0.74$. In addition, the diffusion model will no longer be valid for high particle concentrations, where particle-particle interactions become significant.

At the highest stable intensity shown in Fig. 4, the maximum concentration is only 0.06, which is still within the regime where multiple scattering can be neglected for significant propagation lengths. For the conditions of the above example, the optical mean free path is 1 cm [9], and thus stable POST phenomena can be observed before scattering losses become a factor. The ratio between the effective nonlinear Kerr coefficient and the optical losses should be high to demonstrate nonlinear effects before the onset of loss. It has been shown that this ratio is particularly high when using dielectric spheres as an artificial Kerr medium [4]. The characteristically small perturbations in particle concentration also enable simplifications that are convenient from both an analytic as well as an applications perspective. Specifically, the waveguiding impact is dramatic at low particle concentrations, where particle-particle contributions to both transport and scattering may be safely neglected.

In the context of microfluidic-based photonic applications, the waveguide effect resulting from relatively dilute particle self-focusing represents inherent sensitivity. POST formation and intensity are readily detectable, while depending critically on particle characteristics of interest, including refractive index and size. For instance, the sensitivity of peak intensity to input power scales with the cube of the particle radius. In addition, the fluid nature of POST presents multiple opportunities for photonic devices and research, such as self-formed dynamic optical waveguide networks.

In summary, we have studied self-trapping for a mutually coupled particle-optical system. The analytic self-trapped solution is accurate for low powers and was extended in this work by a numerical solution for higher powers. The numerical solution demonstrated the time-dependent evolution to a self-trapped waveguide. An insensitivity to initial beam geometry was observed. Furthermore, a stability limit was found on the order of a defined critical optical intensity I_0. This analysis shows the potential, and the limitations, of self-trapped waveguiding for optofluidic applications.

[1] G. I. Stegeman and M. Segev, Science **286**, 1518 (1999).
[2] R. Y. Chiao, E. Garmire, and C. H. Townes, Phys. Rev. Lett. **13**, 479 (1964).
[3] M. Segev, B. Crosignani, A. Yariv, and B. Fischer, Phys. Rev. Lett. **68**, 923 (1992).
[4] P. W. Smith, P. J. Maloney, and A. Ashkin, Opt. Lett. **7**, 347 (1982).
[5] K. C. Neuman and S. M. Block, Rev. Sci. Instrum. **75**, 2787 (2004).
[6] A. Ashkin, J. M. Dziedzic, and P. W. Smith, Opt. Lett. **7**, 276 (1982).
[7] V. E. Yashin, S. A. Chizhov, R. L. Sabirov, T. V. Starchikova, N. V. Vysotina, N. N. Rozanov, V. E. Semenov, V. A. Smirnov, and S. V. Fedorov, Opt. Spectrosc. **98**, 511 (2005).
[8] D. Psaltis, S. R. Quake, and C. Yang, Nature (London) **442**, 381 (2006).
[9] R. S. Conroy, B. Mayers, D. V. Vezenov, D. B. Wolfe, M. G. Prentiss, and G. M. Whitesides, Appl. Opt. **44**, 7853 (2005).
[10] M. Brambilla, L. A. Lugiato, F. Prati, L. Spinelli, and W. J. Firth, Phys. Rev. Lett. **79**, 2042 (1997).
[11] W. Singer, M. Frick, S. Bernet, and M. Ritsch-Marte, J. Opt. Soc. Am. B **20**, 1568 (2003).
[12] A. W. Snyder and D. J. Mitchell, Opt. Lett. **18**, 101 (1993).